Journal of Neonatal Surgery
ISSN(Online): 2226-0439
Vol. 14, Issue 15s (2025)
https://www.jneonatalsurg.com

OPEN ACCESS

Efficient Algorithm for Optic Disc Segmentation in Retinal Images

Subham Shome[1], Radhika Mandawewala[2], Subhasish Roy[3], Anirban Mitra[4*], Subrata Paul[5], Amitava Podder[6], Stobak Dutta[7]

[1]Autonomous University of Madrid, Madrid, Spain

[2]Accenture, New Town, Kolkata, India

[3,4]Amity University Kolkata, New Town, India

0000-0001-9543-8977, 0000-0002-6639-4407

[5,6]Department of CSE-AI, Brainware University, Barasat, 700125, West Bengal, India

0000-0001-5920-0654, 0009-0004-9268-3781

[7]Department of CSE, St Thomas' College of Engineering and Technology, Kidderpore, 700023, West Bengal, India.

0000-0002-7719-7812

***Corresponding Author:**

Email ID: amitra@kol.amity.edu

Cite this paper as: Subham Shome, Radhika Mandawewala, Subhasish Roy, Anirban Mitra, Subrata Paul, Amitava Podder, Stobak Dutta, (2025) Efficient Algorithm for Optic Disc Segmentation in Retinal Images. *Journal of Neonatal Surgery*, 14 (15s), 201-209.

ABSTRACT

Segmentation of the optic disc from retinal fundus images is a crucial step within various algorithms aimed at detecting eye pathologies like glaucoma and diabetic retinopathy. Accurate segmentation of the optic disc is vital for the automatic detection of such pathologies. In this study, we present a simple yet highly effective approach for segmenting optic discs from retinal fundus images. Our objective is to provide an uncomplicated yet robust segmentation method that can be executed swiftly. We propose an algorithm that leverages fundamental image processing principles, specifically thresholding in conjunction with morphological operations, to accomplish optic disc segmentation. Despite its reliance on basic image processing techniques, our algorithm yields exceptional effectiveness while demanding minimal computational time. The evaluation of our approach utilizes the well-known publicly available Drishti-GS dataset. The evaluation of our segmentation algorithm produced compelling results, achieving a Sørensen-Dice coefficient of 93.95%, a Jaccard index of 88.9%, precision of 99.67%, recall of 99.89%, and a Matthews Correlation Coefficient of 94%. Additionally, the accuracy of the localized centers within the final segmentation masks was measured using the Euclidean distance, resulting in an accuracy of 99.67%. Notably, our algorithm was executed on the complete Drishti-GS dataset, encompassing 101 images. This study introduces a straightforward yet highly effective approach for optic disc segmentation in retinal fundus images. The algorithm's reliance on basic image processing operations does not compromise its performance, as evidenced by the exceptional evaluation metrics achieved. These outcomes underscore the significance of our proposed method in facilitating the automatic detection of various eye pathologies. The efficiency of our approach, along with its promising results, suggests its potential application in broader medical image analysis contexts.

Keywords: *image processing, biomedical imaging, retinal fundus image, optic disc, segmentation, localization.*

1. INTRODUCTION

The segmentation of the optic disc plays a crucial role in numerous algorithms designed for the detection of eye pathologies, including glaucoma and diabetic retinopathy. Accurate segmentation of the optic disc is of paramount importance for the automatic detection and diagnosis of these pathologies. The optic disc, also known as the optic nerve head, is the anatomical structure where the optic nerve enters the eye. Figure-1 shows a labelled retinal fundus image with the optic disc marked in it (Haggstrom, 2014). It serves as a gateway for the transmission of visual information from the retina to the brain. Its accurate segmentation is vital for assessing the overall health of the eye and detecting potential abnormalities that may be indicative of ocular pathologies. In recent years, numerous computer-aided diagnostic systems have been developed to automate the analysis of retinal images for early detection and monitoring of eye diseases. Among these systems, optic

disc segmentation is a fundamental step, as it provides a region of interest (ROI) within which subsequent analysis can be performed. By precisely delineating the optic disc boundary, cliniciansandresearchers gain valuable insights into the structural and vascular changes associated with various ocular diseases.

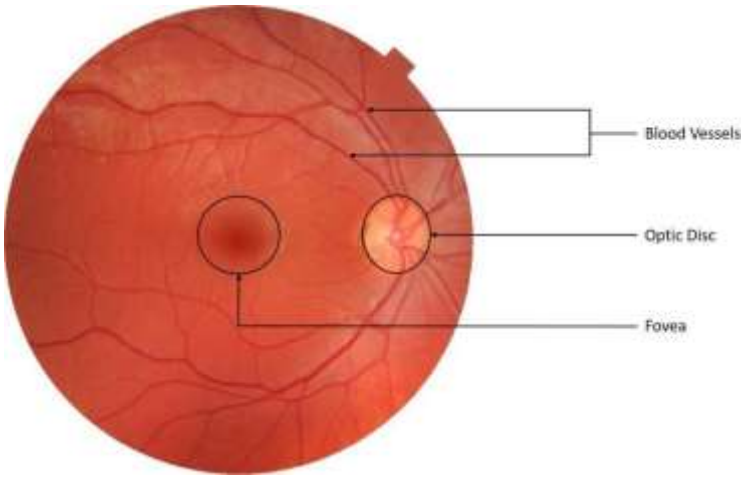

Figure 1. A manually labelled retinal fundus image showing the position of the optic disc

While several sophisticated segmentation techniques have been proposed in the literature, many of them are computationally demanding and require extensive computational resources. Furthermore, their complexity often hampers their practical adoption in resource-limited settings, hindering their widespread use in clinical practice. Therefore, there is a growing demand for efficient and straightforward algorithms that strike a balance between segmentation accuracy and computational efficiency.

In this paper, we present a novel approach to optic disc segmentation that leverages basic image processing operations, namely thresholding and morphological operations. The proposed algorithm is specifically designed to achieve accurate segmentation while minimizing computational requirements. By exploiting the inherent characteristics of retinal fundus images and the distinct properties of the optic disc, our method effectively identifies and delineates the optic disc region, thus facilitating subsequent analysis and pathology detection.

2. To evaluate the performance of our approach, we employ the publicly available Drishti-GS dataset, which is widely recognized as a benchmark for optic disc segmentation. By comparing our results against ground truth annotations provided in the dataset, we demonstrate the effectiveness and reliability of our algorithm in accurately segmenting the optic disc. The contributions of this paper are threefold: Firstly, we introduce a simple yet effective approach for optic disc segmentation, emphasizing the use of basic image processing principles. Secondly, we achieve exceptional segmentation accuracy on the challenging Drishti-GS dataset, demonstrating the robustness and generalizability of our method. Finally, our algorithm exhibits remarkable computational efficiency, making it suitable for real-time applications and resource constrained environments.

3. LITERATURE REVIEW

Various approaches have been proposed for optic disc segmentation, encompassing both traditional image processing methods and state-of-the-art deep learning techniques. Traditional image processing methods have been widely used for optic disc segmentation due to their simplicity and low computational cost. These methods often involve basic operations like thresholding, edge detection, and morphological operations. Bhat & Kumar (2018) proposed a method based on the Hough transform and morphological operations to identify the optic disc's boundary. Similarly, Zheng et al. (2013) employed a combination of thresholding and active contour models for optic disc segmentation. While these techniques have shown promising results, they may struggle with complex or noisy datasets.

Deep learning methods, particularly Convolutional Neural Networks (CNNs), have demonstrated remarkable performance in optic disc segmentation tasks. Fu et al. (2021) utilized a U-Net architecture for accurate optic disc segmentation from retinal images. Deep learning methods often require large labeled datasets for training, making them more computationally demanding and resource-intensive compared to basic image processing approaches. In the realm of retinal image analysis, several research studies have explored different techniques for localization and detection of key structures to aid in the diagnosis of diseases like glaucoma. Niemeijer et al. (2009) addressed retinal image structure localization issues and utilized a KNN regression approach to predict image pixel distances to specific object positions based on image features. However, the lack of optimization for the k value hindered obtaining an optimal solution, leading to confusion in the pixel distance-based approach. Therefore, the need to determine a suitable distance metric to optimize the results and balance recognition performance arose.

Del Rincon et al. (2014) presented an automated glaucoma detection approach that involved image processing techniques, such as noise removal and illumination variation correction. Their method utilized Isotropic Undecimated Wavelet Transform (IUWT) and adaptive thresholding to generate blood vessel masks for locating the disc and cup area. Despite these efforts, challenges remained in segmentation, particularly in the presence of blood vessel occlusions, low contrast, and illumination variation, limiting the effectiveness of the final glaucoma screening process. Harangi & Hajdu (2015) focused on enhancing optic disc (OD) localization by combining multiple prediction methods. Their approach achieved improved OD discovery performance concerning precision and accuracy ratios. However, the use of likelihood maps during the recognition process posed test-time challenges, being computationally intensive and one-sided. Visual assessment in certain cases depended on a priori knowledge and limited capabilities to distinguish subtle differences and describe new imaging markers (Gillies et al., 2016). To overcome these limitations, Machine Learning (ML), radiomics, and Deep Learning (DL) techniques have been proposed to increase quantitative data, reduce inter-reader variations, enhance prognostic and diagnostic accuracy, and minimize biases and subjectivity (Kolossváry et al., 2015).

Nonetheless, some methods, like Convolutional Neural Networks (CNN), remained computationally expensive (Dos Santos Ferreira et al., 2018). Mvoulana et al., (2019) introduced a fully automated approach for glaucoma screening and diagnosis using retinal fundus images. Their method involved OD detection through template matching and the brightness criterion approach, followed by model and texture-based segmentation for extracting OD and OC. Healthy and glaucomatous patients were classified based on the CDR, achieving an impressive 98% accuracy for glaucoma diagnosis. The researchers planned to explore deep learning methods to further improve early glaucoma screening.

Researchers have also utilized artificial intelligence techniques for disease diagnosis in various medical imaging areas. Khan et al. (2020) proposed a fully automated system using deep learning to extract image features. Similarly, Veena et al. (2022) employed curvelet transformation and Ant Colony Optimization for feature extraction, followed by SVM classification. Majid et al., (2020) utilized CNN and Genetic Algorithm for feature selection, but the combination of methods might lead to feature loss. Rehman et al. (2020) designed an automated system using filters and Histogram Oriented Gradient (HOG) for feature extraction and SVM with a cubic kernel for image classification. However, minute features could be lost using this approach. The Drishti-GS dataset has emerged as a popular benchmark for evaluating optic disc segmentation algorithms. Researchers have proposed several techniques using this dataset to achieve high segmentation accuracy. Zhang et al. (2019) highlights a novel approach named Edge-attention guidance Network (ET-Net), designed to enhance segmentation accuracy by incorporating edge information. Wang et al. (2019) introduces a novel framework called pOSAL (patch-based Output Space Adversarial Learning), designed to robustly segment OD and OC across diverse fundus image datasets. To overcome the limitations of domain shift in neural networks, pOSAL integrates a lightweight segmentation network as a backbone and employs a morphology-aware segmentation loss for precise results. Kamble et al. (2020) introduced a combined analysis approach for detecting retinal structures, presenting a novel method using U-Net++ and EfficientNet-B4 to accurately segment optic disc, cup, and fovea.

1. Dataset

The research utilized the Drishti-GS dataset (Sivaswamy et al., 2014), a comprehensive and diverse collection of eye gaze data, for training and testing. The dataset comprises a total of 101 images, with 50 images allocated for training and 51 images for testing and the training set is accompanied by ground truth annotations. The data acquisition process has been elaborated in the following sections.

3.1 Original Image Acquisition

All 101 images in the DRISHTI-GS dataset (Liu et al., 2021) were obtained from visitors to the Aravind Eye Hospital in Madurai (TN, India), with their informed consent. Clinical investigators selected patients with glaucoma based on their clinical examination findings. The chosen patients represented a range of ages (40-80 years) and had an approximately equal distribution of males and females. Additionally, individuals without glaucoma who were undergoing routine refraction tests were selected to represent the normal class. During data collection, all images were captured with dilated pupils following a specific protocol. The images were centered on the optic disc (OD) with a Field-of-View of 30-degrees. The images were of high resolution, with dimensions of 2896 × 194*A* pixels and saved in PNG uncompressed format. No other restrictions were imposed on the image acquisition process.

3.2 Ground Truth Collection

To ensure accurate annotations, ground truth markings were obtained for each image from four glaucoma experts with varying years of experience (3, 5, 9, and 20 years). This allowed for capturing the inter-observer variability in the markings. Images of poor quality, such as those with low contrast or mis-positioned OD regions, were discarded. In this dataset release, the original images were further processed by extracting the fundus region, which contains retinal structures, by removing the surrounding non-fundus black regions. This resulted in images of approximately 2047 × 1760 pixels in size. In order to achieve precise boundary marking for irregular shapes of the optic disc (OD) and cup regions, a dedicated marking tool was developed. This tool allowed human experts to accurately mark the boundaries by utilizing a deformable

circle with multiple control points. The marking process involved positioning the circle close to the approximate boundary and then refining the fit by adjusting individual control points. This two-step approach enabled accurate shape marking, capturing both the overall localization and local deformations of the regions of interest. In this research, only the optic disc (OD) data (image and ground truth) were utilized.

4. METHODOLOGIES

In this section, we outline the step-by-step methodology employed for accurate segmentation and analysis of blood vessels in images. The methodology encompasses several stages, each contributing to the refinement and evaluation of the segmentation results.

Pre-processing: Initial preparation of the input image involves loading the image, extracting the red channel, applying intensity thresholding, cropping the region of interest, and enhancing contrast for subsequent analysis.

Conditional Thresholding: Conversion of the adjusted red channel image to a binary image through conditional thresholding, involving empirically determined thresholds based on calculated ratios.

Morphological Operations: Application of morphological operations to refine the segmented binary image, including preserving the largest connected component and performing a closing operation.

Post-processing: Modifying the binary image through padding to match the dimensions of the original input image, ensuring accurate analysis and comparison.

Calculation of Center Points: Computation of centroids of segmented objects for accuracy evaluation through comparison with ground truth data, utilizing Euclidean distance as a metric and generating boundary masks for visual assessment. Figure-2 provide a visual representation of the procedure steps.

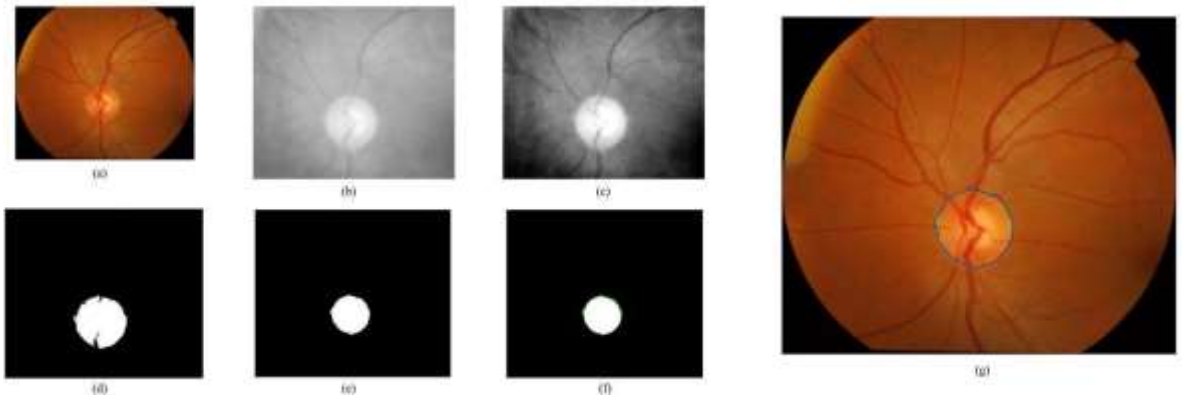

Figure 2. Steps taken to perform the OD segmentation with the final score on one image from the dataset. A. Original image B. Cropped red channel C. Contrast enhanced image D. Thresholded image E. Thresholded image with largest connected pixels, reverted to original size F. Comparison with ground truth G. Result (blue - proposed method, green- ground truth)

4.1 Pre-processing

The pre-processing stage in the methodology begins by loading the input image and ground truth data. The image is loaded using the specified filename, and the red channel is extracted from the image. This step focuses on the red channel as it contains relevant information related to the blood vessels. After extracting the red channel, the intensity values below a threshold of 20 are set to 0. This thresholding operation helps to remove darker regions from the image, reducing noise and highlighting the blood vessels. To further refine the analysis and focus on the region of interest, a cropping window is defined.

Since the input image may contain irrelevant areas outside the region of interest, cropping the image to a smaller size can help focus the analysis on the blood vessel region. In this step, a cropping window is defined based on a target size, which is calculated as a percentage of the original image dimensions. The target size for cropping is calculated as 75% of the image dimensions. The cropping window specifies the region of interest within the image. It is then applied to both the red channel image and the original image, resulting in cropped versions of these images. To enhance the contrast of the cropped red channel image, contrast adjustment is applied. This step helps to further improve the visibility of the blood vessels and facilitate subsequent segmentation. The pre-processing stage involves loading the image and ground truth data, extracting the red channel, applying intensity thresholding, cropping the images to the region of interest, and enhancing the contrast of

the cropped red channel image. These steps prepare the data for the subsequent segmentation process.

4.2 Conditional Thresholding

In order to perform segmentation on the red channel image, it is necessary to convert it into a binary image. This is achieved through a thresholding operation on the adjusted red channel image. Pixels with intensity values above a certain threshold are assigned a value of 1, indicating the presence of blood vessels, while pixels with intensity values below the threshold are assigned a value of 0. In this case, conditional thresholding is applied to obtain a binary image from the adjusted red cropped image. The threshold value is determined based on the calculated ratio. If the ratio falls within the range of 0.07 to 0.1, a threshold of 210 is selected. For ratios between 0.1 and 0.22, the threshold is set to 218. Similarly, if the ratio falls between 0.22 and 0.3, the threshold value is set to 230. In cases where the ratio exceeds 0.3, the threshold is set to 215. These values were measured empirically. Using the selected threshold, the binary image is obtained by comparing the adjusted red cropped image with the threshold value.

4.3 Morphological Operations

Following the thresholding step, additional morphological operations are employed to refine the segmented binary image. First, the largest connected component in the image is preserved while eliminating smaller noise regions. This is achieved by selectively retaining the component with the greatest area. Subsequently, a morphological closing operation (Equation-1) is performed to further refine the segmentation result. A disk-shaped structuring element with a radius of 100 pixels is used for this purpose. The closing operation aims to bridge any gaps present in the binary image and produce a smoother boundary for the segmented object.

$$f \cdot s = (f \otimes s_{rot}) \ominus s_{rot} \dots\dots\dots\dots\dots\dots\dots (1)$$

By applying these morphological operations, the segmentation accuracy is enhanced, ensuring the removal of noise and the improvement of object boundaries in the binary image.

4.4 Post-processing

post-processing stage, the binary image obtained from the previous steps is padded to match the dimensions of the original input image. This ensures that the segmented binary image aligns properly with the original image for accurate analysis and comparison. To determine the amount of padding required, the remaining rows and columns after cropping are calculated. This is done by subtracting the limits of the cropped region from the total number of rows and columns in the original image. The binary image is then padded with zeros on the left and top sides to adjust its size. This padding operation adds zeros before the existing content of the image, aligning it with the original image. Subsequently, the padded binary image is extended on the right and bottom sides to match the dimensions of the original image. This ensures that the binary image retains the same size as the input image, accommodating any additional pixels needed. By performing these padding operations, the binary image is modified to match the size of the original input image. This enables consistent analysis and accurate comparison between the segmented regions and the corresponding regions in the original image.

4.5 Calculation of Center points

In the subsequent step of the methodology, the centroids of the segmented objects are computed and compared with the corresponding ground truth data. This analysis is conducted to evaluate the accuracy of the segmentation results. To determine the centroids of the segmented regions, their coordinates are extracted from the binary image. The obtained centroid coordinates are compared with the ground truth center point. In order to assess the accuracy of the centroid estimation, the Euclidean distance between the calculated centroids and the ground truth center point is computed. The Euclidean distance serves as a measure of dissimilarity between the estimated and ground truth centroids. To provide a reference scale for the Euclidean distance, the diagonal distance of the image is calculated. This diagonal distance represents the maximum possible distance within the image. By utilizing the Euclidean distance and the diagonal distance, the distance accuracy is evaluated. This accuracy metric quantifies the agreement between the estimated centroids and the ground truth center point. To facilitate the visualization of the segmentation results, boundary masks are generated. These masks outline the boundaries of the segmented objects in the original and cropped images, allowing for a visual assessment of the segmentation performance and a direct comparison with the ground truth data.

5. RESULTS AND DISCUSSION

The full Drishti-GS dataset, which contains a total of 101 images, was tested with the algorithm. NVIDIA GeForce GTX 1650 graphics was used for performing the operations.

5.1 Optic Disc Segmentation Results

Various evaluation metrics were used for getting the accuracy of the algorithm. The details are elaborated in the following sections.

Sørensen-Dice Coefficient: This is one of the most commonly used evaluation method for finding image segmentation. It is

essentially given by the Equation-2, for an overlap of two binary images as shown in Figure-3 (Chrastek et al., 2005).

$$DSC = \frac{2|X \cap Y|}{|X|+|Y|} \ldots\ldots\ldots\ldots\ldots\ldots\ldots\ldots (2)$$

where, *X* and *Y* are the two binary masks for the predicted and actual images for the Optic Discs.

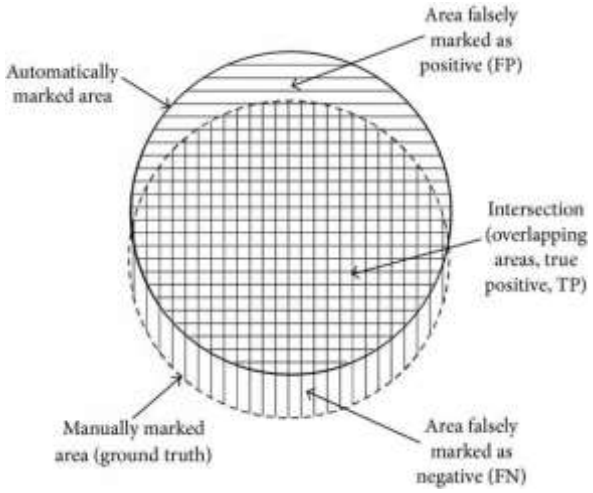

Figure 3. Result Metrics for Image Segmentation

Jaccard Index: This is another popular image segmentation evaluation metric. This is given by Equation-3 for two over lapping binary images.

$$I = \frac{|X \cap Y|}{|X \cup Y|} = \frac{|X \cap Y|}{|X|+|Y|-|X \cap Y|} \ldots\ldots\ldots\ldots\ldots\ldots (3)$$

where, *X* and *Y* are the two binary masks for the predicted and actual images for the Optic Discs.

Precision and Recall: These two are the most commonly used evaluation metric for any general problem of prediction, and also for segmentation. The binary confusion matrix is first created based on Figure-1 and then, the four values in the confusion matrix viz. True Positive (TP), False Positive (FP), False Negative (FN) and True Negative (TN) are extracted. From these values, Precision and Recall are given by Equation-4 and Equation-5 respectively.

$$Precision = \frac{TP}{(TP + FP)} \ldots\ldots\ldots\ldots\ldots\ldots\ldots\ldots (4)$$

$$Recall = \frac{TP}{(TP + FN)} \ldots\ldots\ldots\ldots\ldots\ldots\ldots\ldots\ldots\ldots (5)$$

One thing to point out here is that we did not consider accuracy, which is given by (*TP + TN)/imageSize*, as a measure of evaluation, since the value of True Negative (TN) will be very high and it will thus increase the accuracy falsely. Figure-4 shows the result provided by the algorithm on randomly chosen images from the dataset.

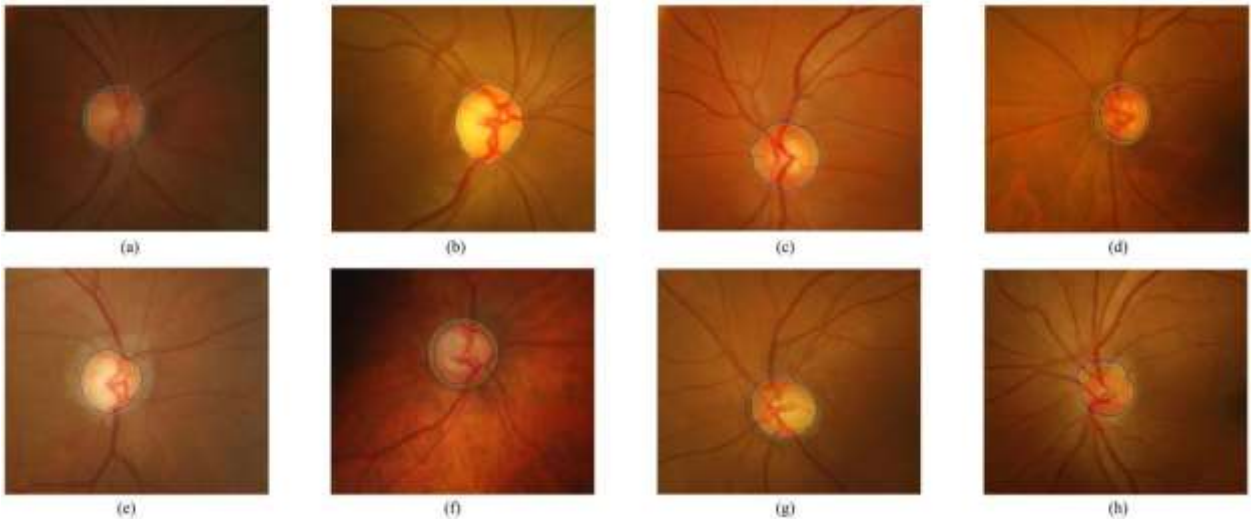

Figure 4. Sørensen-Dice Coefficient result of OD segmentation results on various images from the dataset. A. 0.97311 B. 0.97895 C. 0.97062 D. 0.91237 E. 0.96751 F. 0.82915 G. 0.97123 H. 0.88859

Matthews Correlation Coefficient: The Matthews Correlation Coefficient (Chicco et al., 2021) provides a comprehensive view of the classifier's performance, and this was used for our last segmentation evaluation metric, considering the True Negative (TN) into account. This was primarily used since Precision and Recall cannot take into account TN for calculation. This is given by Equation-6 and provides one of the best measures of segmentation.

$$MCC = \frac{(TP \times TN - FP \times FN)}{\sqrt{(TP + FP)(TP + FN)(TN + FP)(TN + FN)}} \ldots\ldots\ldots\ldots\ldots\ldots (6)$$

Along with DSC and JI, MCC provides a very high correctness of evaluation metric calculation for image segmentation. The comparison of all the segmentation evaluation metrics is given in Figure-5 and the values are shown in Table-1.

Table 1. Optic Disc Segmentation Results

2. Evaluation Metric	**3. Mean**	**4. STD**
5. Sørensen-Dice Coefficient	6. 0.9395	7. 0.0452
8. Jaccard Index	9. 0.889	10. 0.0744
11. Precision	12. 0.9967	13. 0.0024
14. Recall	15. 0.9989	16. 0.0015
17. F_1-score	18. 0.9979	19. 0.0018
20. Matthews Correlation Coefficient	21. 0.94	22. 0.0422

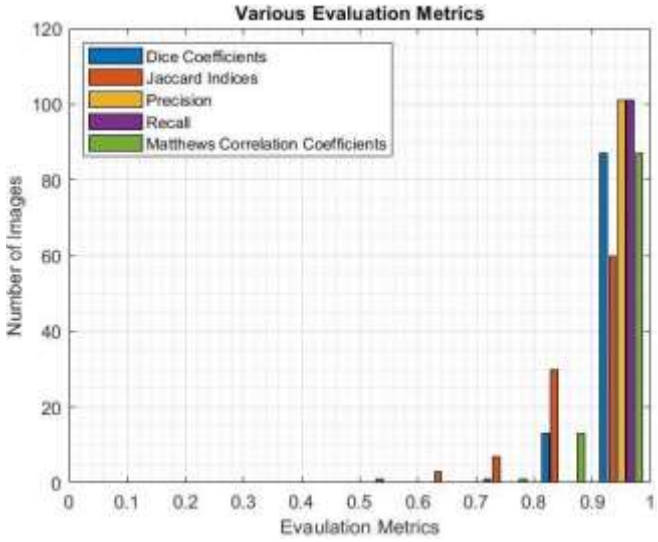

Figure 5. Optic Disc Segmentation Evaluation Results

5.2 Center Localization Results

The localization of centers of optic disc was calculated using the Euclidean distance between the ground truth pixel coordinates and predicted pixel coordinates.

Euclidean Distance: The Euclidean distance is by far the most commonly used performance measure for calculation of accuracy of coordinates. It is given by Equation-7.

$$d = \sqrt{(x_2 - x_1)^2 + (y_2 - y_1)^2} \quad \ldots\ldots (7)$$

where, (x_1, x_2) and (y_1, y_2) are the predicted and ground truth pixel coordinates respectively. The final accuracy is calculated as a ratio of d and the longest distance between any two points on the image, which is essentially any one of the two diagonals of the image. Hence, the final localization accuracy is given by Equation-8.

$$Localization = \frac{d}{diagonal} \quad \ldots\ldots (8)$$

The result of OD Center Localization is given in Figure-6 and the value is shown in Table-2.

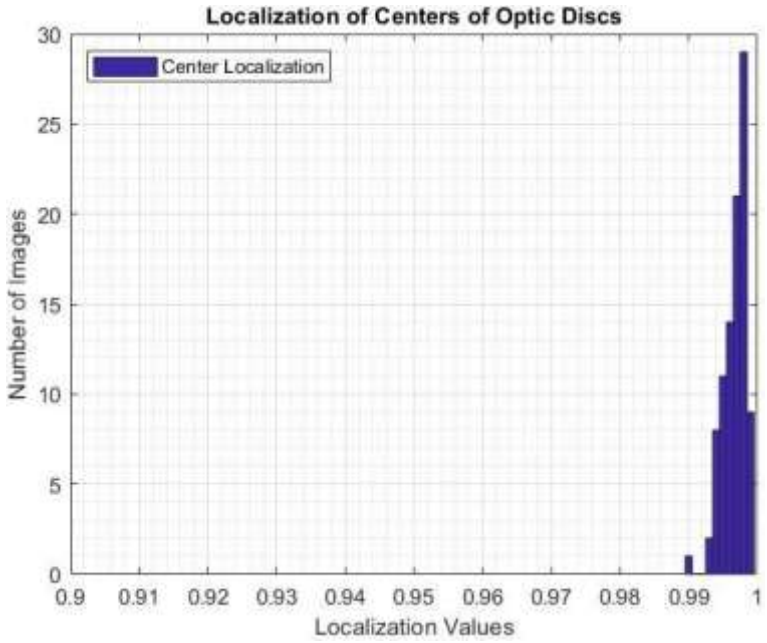

Figure 6. OD Center Localization Results

Table 2. Optic Disc Center Localization Results

23.	24. Mean	25. STD
26. Euclidean Localization	27. 0.9967	28. 0.0025

6. CONCLUSION

In this study, we have presented a straightforward yet highly effective approach for the segmentation of optic discs from retinal fundus images using basic image processing principles. The accurate identification of optic discs is pivotal in various algorithms aimed at detecting eye pathologies like glaucoma and diabetic retinopathy. Our proposed algorithm relies on a sequence of simple image processing operations, namely thresholding and morphological operations, which collectively demonstrate exceptional performance with minimal computational overhead. By employing our methodology on the renowned Drishti-GS dataset, we achieved remarkable results in optic disc segmentation. The evaluation metrics indicate the algorithm's robustness and precision, with a Sørensen-Dice coefficient of 93.95%, a Jaccard index of 88.9%, a precision rate of 99.67%, and a recall rate of 99.89%. Furthermore, the Matthews Correlation Coefficient of 94% reinforces the algorithm's overall effectiveness. Our technique for center localization also demonstrated a high accuracy of 99.67%, further validating the reliability of our approach. The application of conditional thresholding and morphological operations in our methodology aids in refining the segmented binary images, successfully eliminating noise and enhancing object boundaries. Moreover, our post-processing steps, including padding and resizing, ensure consistency and accuracy in the analysis and comparison of segmented regions with their corresponding regions in the original images. The calculated centroids of segmented objects, alongside the Euclidean distance analysis, provide a comprehensive assessment of segmentation accuracy. Additionally, the generation of boundary masks facilitates a visual evaluation of the segmentation performance and allows for direct comparison with ground truth data. Our proposed algorithm showcases a remarkable balance between simplicity and efficacy, making it a valuable contribution to the field of biomedical image processing. The impressive results obtained on the Drishti-GS dataset underline its potential for aiding in the automated detection of eye pathologies. As future work, this approach could be extended to broader datasets and further refined to accommodate diverse retinal conditions, thereby advancing the diagnostic capabilities in ophthalmology.

REFERENCES

[1] Haggstrom, M. (2014). Medical gallery of Mikael Haggstrom 2014. Wikijournal of Medicine, 1(2). https://doi.org/10.15347/WJM/2014.008

[2] Bhat, S. H., & Kumar, P. (2018). Segmentation of optic disc by localized active contour model in retinal fundus image. In Smart Innovations in Communication and Computational Sciences: Proceedings of ICSICCS-2018 (pp. 35–44).

[3] Zheng, Y., Stambolian, D., O'Brien, J., et al. (2013). Optic disc and cup segmentation from color fundus photograph using graph cut with priors. In Medical Image Computing and Computer-Assisted Intervention–MICCAI 2013: 16th International Conference (pp. 75–82). Springer.

[4] Fu, Y., Chen, J., Li, J., et al. (2021). Optic disc segmentation by U-Net and probability bubble in abnormal fundus images. Pattern Recognition, 117, 107971. https://doi.org/10.1016/j.patcog.2021.107971

[5] Niemeijer, M., Abramoff, M. D., & Van Ginneken, B. (2009). Fast detection of the optic disc and fovea in color fundus photographs. Medical Image Analysis, 13(6), 859–870.

[6] Del Rincon, A. G. J. M., Miller, P., & Blanco, A. A. (2014). Automatic analysis of digital retinal images for glaucoma detection. In Irish Machine Vision and Image Processing Conference, Derry, United Kingdom.

[7] Harangi, B., & Hajdu, A. (2015). Detection of the optic disc in fundus images by combining probability models. Computers in Biology and Medicine, 65, 10–24.

[8] Gillies, R. J., Kinahan, P. E., & Hricak, H. (2016). Radiomics: Images are more than pictures, they are data. Radiology, 278(2), 563–577.

[9] Kolossváry, E., Ferenci, T., Kováts, T., et al. (2015). Trends in major lower limb amputation related to peripheral

arterial disease in Hungary: A nationwide study (2004–2012). European Journal of Vascular and Endovascular Surgery, 50(1), 78–85.

[10] Dos Santos Ferreira, M. V., Carvalho Filho, A. O., De Sousa, A. D., et al. (2018). Convolutional neural network and texture descriptor-based automatic detection and diagnosis of glaucoma. Expert Systems with Applications, 110, 250–263.

[11] Mvoulana, A., Kachouri, R., & Akil, M. (2019). Fully automated method for glaucoma screening using robust optic nerve head detection and unsupervised segmentation-based cup-to-disc ratio computation in retinal fundus images. Computerized Medical Imaging and Graphics, 77, 101643.

[12] Khan, M. A., Ashraf, I., Alhaisoni, M., et al. (2020). Multimodal brain tumor classification using deep learning and robust feature selection: A machine learning application for radiologists. Diagnostics, 10(8), 565.

[13] Veena, H., Muruganandham, A., & Kumaran, T. S. (2022). A novel optic disc and optic cup segmentation technique to diagnose glaucoma using deep learning convolutional neural network over retinal fundus images. Journal of King Saud University - Computer and Information Sciences, 34(8), 6187–6198.

[14] Majid, A., Khan, M. A., Yasmin, M., et al. (2020). Classification of stomach infections: A paradigm of convolutional neural network along with classical features fusion and selection. Microscopy Research and Technique, 83(5), 562–576.

[15] Rehman, A., Khan, M. A., Mehmood, Z., et al. (2020). Microscopic melanoma detection and classification: A framework of pixel-based fusion and multilevel features reduction. Microscopy Research and Technique, 83(4), 410–423.

[16] Zhang, Z., Fu, H., Dai, H., et al. (2019). ET-Net: A generic edge-attention guidance network for medical image segmentation. In Medical Image Computing and Computer-Assisted Intervention – MICCAI 2019, Part I(22), 442–450. Springer.

[17] Wang, S., Yu, L., Yang, X., et al. (2019). Patch-based output space adversarial learning for joint optic disc and cup segmentation. IEEE Transactions on Medical Imaging, 38(11), 2485–2495.

[18] Kamble, R., Samanta, P., & Singhal, N. (2020). Optic disc, cup and fovea detection from retinal images using U-Net++ with EfficientNet encoder. In Ophthalmic Medical Image Analysis: 7th International Workshop (pp. 93–103). Springer.

[19] Sivaswamy, J., Krishnadas, S., Joshi, G. D., et al. (2014). Drishti-GS: Retinal image dataset for optic nerve head (ONH) segmentation. In 11th IEEE International Symposium on Biomedical Imaging (ISBI) (pp. 53–56).

[20] Liu, B., Pan, D., & Song, H. (2021). Joint optic disc and cup segmentation based on densely connected depth-wise separable convolution deep network. BMC Medical Imaging, 21(1), 14. https://doi.org/10.1186/s12880-020-00528-6

[21] Chrastek, R., Wolf, M., Donath, K., Niemann, H., Paulus, D., Hothorn, T., et al. (2005). Automated segmentation of the optic nerve head for diagnosis of glaucoma. Medical Image Analysis, 9(4), 297–314.

[22] Chicco, D., Totsch, N., & Jurman, G. (2021). The Matthews correlation coefficient (MCC) is more reliable than balanced accuracy, Bookmaker informedness, and markedness in two-class confusion matrix evaluation. BioData Mining, 14(1)